Zhou *et al. Energy Mater.* **2025**, *5*, 500010
DOI: 10.20517/energymater.2024.64

Energy Materials

Article

Open Access

Check for updates

Enhanced photodegradation of ciprofloxacin with organic photocatalyst through a ternary strategy

Yang Zhou[1,#], Ciyuan Huang[1,#], Linji Yang[1,#], Ruirui Zhang[1,2], Yanzhen Yin[2,*], Cong Liu[1], Ke Sun[3], Shangfei Yao[1], Nannan Geng[1], Yu Luo[5], Tao Yang[4], Bingsuo Zou[1], Tao Liu[1,3,*]

[1]School of Chemistry and Chemical Engineering, State Key Laboratory of Featured Metal Materials and Life-cycle Safety for Composite Structures, School of Resources, Environment and Materials, Guangxi University, Nanning 530004, Guangxi, China.
[2]Guangxi Key Laboratory of Green Chemical Materials and Safety Technology, Beibu Gulf University, Qinzhou 535000, Guangxi, China.
[3]Department of Biochemistry and Cell Biology, Youjiang Medical University for Nationalities, Baise 533000, Guangxi, China.
[4]Centre for Mechanical Technology and Automation, Department of Mechanical Engineering, University of Aveiro, Aveiro 3810-193, Portugal.
[5]Kennedy Krieger Institute, Johns Hopkins University, Baltimore, MD 21205, USA.
[#]Authors contributed equally.

[*]**Correspondence to:** Prof. Yanzhen Yin, Guangxi Key Laboratory of Green Chemical Materials and Safety Technology, Beibu Gulf University, 12 Binhai Avenue, Binhai New City, Qinzhou 535000, Guangxi, China. E-mail: Yinyinyanzhen2009@163.com; Prof. Tao Liu, School of Chemistry and Chemical Engineering, State Key Laboratory of Featured Metal Materials and Life-cycle Safety for Composite Structures, School of Resources, Environment and Materials, Guangxi University, No.100, Daxue East Road, Nanning 530004, Guangxi, China. E-mail: liutaozhx@gxu.edu.cn

How to cite this article: Zhou, Y.; Huang, C.; Yang, L.; Zhang, R.; Yin, Y.; Liu, C.; Sun, K.; Yao, S.; Geng, N.; Luo, Y.; Yang, T.; Zou, B.; Liu, T. Enhanced photodegradation of ciprofloxacin with organic photocatalyst through a ternary strategy. *Energy Mater.* **2025**, *5*, 500010. https://dx.doi.org/10.20517/energymater.2024.64

Received: 28 Jun 2024 **First Decision:** 26 Jul 2024 **Revised:** 14 Aug 2024 **Accepted:** 20 Aug 2024 **Published:** 8 Jan 2025

Academic Editor: Yuhui Chen **Copy Editor:** Ping Zhang **Production Editor:** Ping Zhang

Abstract

Antibiotics, as emerging organic pollutants, have seriously affected the biodiversity of water and threatened mankind's health. Currently, low charge separation efficiency and insufficient light utilization limit the application of traditional photocatalysts in antibiotic degradation. In this work, the organic photovoltaic material PM6: Y6 was incorporated into an organic photocatalyst with bulk-heterojunction, and a third component, 3,9-bis{2-methylene-[3-(1,1-dicyanomethylene)-cyclopentane-1,3-dione-(c)thiophen]}-5,5,11,11-tetrakis(4-hexylphenyl)-dithieno[2,3-d:2',3'-d']-s-indaceno[1,2-b:5,6-b']dithiophene (ITCPTC), was added to adjust the absorption spectrum of photocatalyst for efficient photodegradation of ciprofloxacin (CIP). Benefiting from excellent light utilization and effective carrier separation and transfer, the catalyst exhibited excellent photocatalytic performance, achieving a 90%/99% degradation rate of CIP within 30/60 min under simulated sunlight irradiation (~79 mW/cm^2). Besides, the catalyst still exhibited good photocatalytic performance after multiple cycles of use. By Electron Spin

Resonance analysis, the active species for photocatalytic degradation of CIP were mainly holes (h^+) and superoxide radicals ($\cdot O_2^-$). Designing photocatalysts with a wider light absorption range and better charge separation is a feasible idea to achieve better photocatalytic performance. It is anticipated that this work could enhance the understanding of modification strategies for ternary organic semiconductors and expand the application of photocatalysis in environmental pollution control and remediation.

Keywords: Organic photocatalyst, ternary strategies, photodegradation, ciprofloxacin

INTRODUCTION

Antibiotics have widespread and long-standing use in modern medicine, while their overuse and delayed metabolism have adverse effects on ecosystems, creating a source of pollution that is difficult to address[1-3]. As emerging organic pollutants, even at low concentrations, they can lead to the multiplication of drug-resistant bacteria, which poses a serious threat to humans[4]. Ciprofloxacin (CIP), a broad-spectrum antibiotic commonly used to treat various bacterial infections, has been found in water sources, agriculture and household waste. Concentrations have now reached 21 μg/L in medical wastewater and up to 5 mg/L in its production wastewater[5,6]. This pollutant is bio-accumulative and non-biodegradable; its removal is important for environmental remediation[7]. Visible light-driven photocatalysis as an advanced oxidation process (AOP) has good application prospects for pollutant degradation[8-10]. Multiphase photocatalysis based on traditional semiconductors such as TiO_2[11-13], ferrite[14], and g-C_3N_4[15,16] has been shown to be effective in degrading antibiotics[17]. However, their disadvantages such as complicated preparation process and narrow light absorption range are not conducive to the treatment of organic pollutants in medical wastewater[18].

Organic active layers of semiconductors usually comprise polymers or small molecules possessing a conjugated structure, including donors and acceptors. Their efficient and rapid exciton dissociation, tunable energy levels and wide absorption range are favorable for photocatalysis in the visible region and make up for the shortage of traditional photocatalysts[19-21]. The Bulk-Heterojunction (BHJ) structure of organic active layers can form an interpenetrating network, which increases the contact area to the donor and acceptor, and facilitates the diffusion and transmission of excitons[22,23]. However, organic semiconductors are unstable and intolerant to water and oxygen, making their application in water treatment challenging[24].

In this study, we prepared photocatalysts by loading organic semiconductor blend films on coconut shell carbon (CSC). This novel photocatalyst has considerable stability and recyclability after loading, making it suitable for use in aquatic environments. Additionally, it combines organic photovoltaics and photocatalysis to achieve excellent results[25-27]. Moreover, incorporating an acceptor named 3,9-bis{2-methylene-[3-(1,1-dicyanomethylene)-cyclopentane-1,3-dione-(c)thiophen]}-5,5,11,11-tetrakis(4-hexylphenyl)-dithieno[2,3-d:2',3'-d']-s-indaceno[1,2-b:5,6-b']dithiophene (ITCPTC) as a third component into the PM6:Y6 system forms ternary blend films, which significantly enhances the photocatalytic performance[28-31]. The ternary system was employed for the photodegradation of CIP. Compared with the binary system, the photocatalytic activity was significantly improved and a 99% removal rate could be realized in 60 min (100 mW/cm^2). Surprisingly, it still achieved 90% degradation of CIP in 60 min under indoor light conditions (1 mW/cm^2), promising to drive practical applications. The enhancement in catalytic performance was primarily attributed to the expanded absorption spectrum of visible light and the improvement in carrier separation efficiency[32-35]. In addition, reactive oxygen species (ROSs) involved in CIP degradation were identified by Electron Spin Resonance (ESR) analysis, indicating that superoxide radicals ($\cdot O_2^-$) and holes (h^+) played important roles. In a word, by innovatively combining photocatalysis and an organic active layer to construct a type-II charge transfer heterojunction, the catalyst not only offers

a wide light absorption range and flexible preparation, but also surmounts the defects of poor stability of organic photovoltaic materials in water, marking a breakthrough in water treatment.

EXPERIMENTAL

Chemicals

CIP, ethylenediaminetetracetic acid disodium (EDTA-2Na, $C_{10}H_{14}N_2Na_2O_8$, 99.0%), 1,4-benzoquinone (BQ) ($C_6H_4O_2$, 98%) and isopropyl alcohol (IPA) (C_3H_8O, 99.7%) were purchased from Aladdin (Shanghai, China). PM6, Y6 and ITCPTC were synthesized in previous articles. All chemicals were directly used without any further processing.

Preparation of immobilized photocatalyst

Preparation of CSC: The collected coconut shells were placed in an electric blast drying oven at 160 °C for three days until they reached a constant weight. The dried coconut shells were mechanically crushed and placed into a tube furnace under N_2 atmosphere and held for 1h to obtain pure CSC.

Preparation of photocatalyst: PM6:Y6: ITCPTC (1:1:0, 1:0:1, 1:0.5:0.5 weight ratio) was loaded on the surface of CSC with a weight ratio of 1:2000. The photocatalyst was denoted as CSC-PM6:Y6: ITCPTC.

Photocatalytic degradation

The characteristics of photocatalysts (CSC-PM6: Y6: ITCPTC) were investigated by degrading CIP under simulated sunlight. The photocatalyst (0.10 g) was dissolved into 50 mL CIP solution (10 mg/L). Before irradiation, the mixture was stirred in the dark for 30min to reach adsorption equilibrium. Photocatalytic experiments were carried out using a Xe lamp light source (CEL-HXF300-T3) AM 1.5G (300~1,100nm) as simulated sunlight. The optical power density at the reactor surface, as measured by the optical power meter, was 79 mW/cm^2. The product after degradation was determined by an ultraviolet-visible (UV-vis) spectrophotometer (SHIMADZU UV-2600i) at 277nm.

RESULTS AND DISCUSSION

Characterization of photocatalysts

The chemical structures of PM6, Y6, and ITCPTC are displayed in Figure 1A. PM6 is a copolymer donor, and Y6 and ITCPTC are small molecule non-fullerene acceptors[36]. The electrochemical cyclic voltammetry (CV) technique was used to measure the highest occupied molecular orbital (HOMO) and lowest unoccupied molecular orbital (LUMO) energy levels of the above materials[37]. After calibration of the reference electrode using ferrocene redox pair (Fc^+/Fc) as an internal reference ratio, the HOMO/LUMO of PM6 is -3.61 eV/-5.50 eV which conforms well to Y6 (-4.10 eV/-5.60 eV) and ITCPTC (-3.95 eV/-5.65 eV)[37,38]. Figure 1B displays the energy level diagram, which is based on the provided data. The energy levels of PM6, Y6, and ITCPTC are intertwined with each other, which facilitates the separation and transfer of charge carriers in BHJ organic semiconductors.

The morphology of the as-prepared CSC-PM6: Y6: ITCPTC was demonstrated by scanning electron microscopy-energy dispersive X-ray spectroscopy (SEM-EDS). As shown in Supplementary Figure 1A and B, CSC has a porous surface structure under the electron microscope, which facilitates the loading of catalysts. The surface morphology of CSC did not change significantly after loading catalysts. In addition, as shown in Supplementary Figure 1C-G, CSC-TiO_2 was prepared in the same way, which destroyed the porous structure of CSC. The EDS spectrum [Supplementary Figure 1H, Supplementary Table 1] revealed the distribution of elements C, O, N, F, and S within the compounds, indicating that the PM6: Y6: ITCPTC and CSC were successfully compounded.

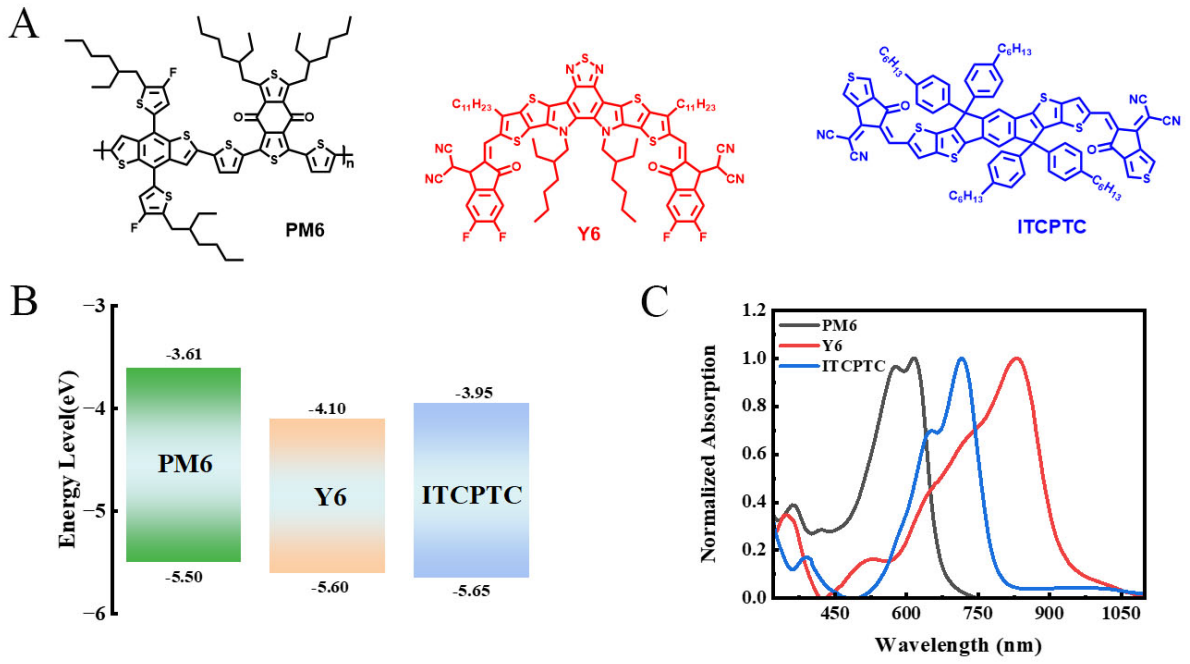

Figure 1. (A) Chemical structures of PM6, Y6 and ITCPTC; (B) Energy level diagrams of PM6, Y6 and ITCPTC; (C) UV-vis DRS of organic semiconductor photocatalyst. UV-vis: Ultraviolet-visible; ITCPTC: 3,9-bis{2-methylene-[3-(1,1-dicyanomethylene)-cyclopentane-1,3-dione-(c)thiophen]}-5,5,11,11-tetrakis(4-hexylphenyl)-dithieno[2,3-d:2′,3′-d′]-s-indaceno[1,2-b:5,6-b′]dithiophene; DRS: Diffuse reflectance spectroscopy.

Considering that the catalyst compounding may affect the specific surface area, the N_2 adsorption-desorption measurements were performed on the catalyst. The N_2 adsorption-desorption isotherms exhibited a IV isotherm with an H_3-type hysteresis loop, and the pore size distribution curves indicated that they have an average pore size of approximately 2 nm [Supplementary Figure 2, Supplementary Table 2], confirming the microporous feature of photocatalyst[39]. The specific surface area (S_{BET}) of CSC (932.52 m^2/g) is larger than that of CSC-PM6: Y6: ITCPTC (894.18 m^2/g). After loading the catalyst, the specific surface area of CSC was slightly reduced and the particle size increased with insignificant changes, which was still beneficial for the progress of interface reactions.

The normalized Ultraviolet Spectroscopy (UV) of materials in pure thin films is shown in Figure 1C; the pure PM6, Y6 and ITCPTC have strong absorption spectra at 500-700 nm, 700-850 nm and 600-750nm, respectively. The absorption peak of ITCPTC lies between those of PM6 and Y6[40]. The absorption spectra between the donor and receptors are complementary, and compounding them is expected to achieve broader absorption in the visible and near-infrared regions. Based on this, we fabricate PM6: Y6: ITCPTC (1:1:0, 1:0:1, 1:0.5:0.5 weight ratio) blend films and prepared photocatalysts. The UV-vis absorption spectra of the blend films are presented in Figure 2A, revealing absorption peaks at 820nm and 717nm in the binary films of PM6:Y6 and PM6: ITCPTC, respectively. After adding a third component, the PM6: Y6: ITCPTC exhibits strong absorption at 600-800 nm. This means that modulating the composition of the third component can broaden the absorption spectrum of photocatalysts.

Next, considering that the third component affects the photoelectric properties of organic photocatalysts, photoluminescence (PL) was conducted to investigate the energy transfer and charge transfer between Y6 and ITCPTC. As shown in Figure 2B, the main emission peaks of ITCPTC are at 780 and 910 nm,

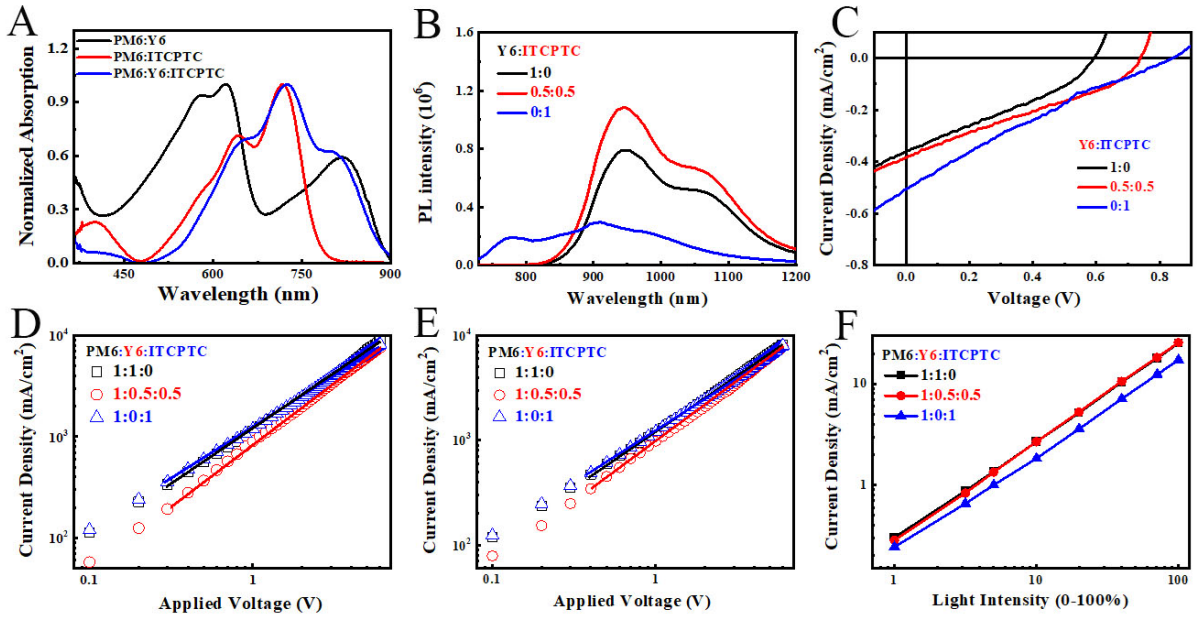

Figure 2. (A) The UV-vis DRS of PM6: Y6:ITCPTC(1:1:0, 1:0:1, 1:0.5:0.5); (B) PL spectra of Y6:ITCPTC and (C) J-V characteristics of Y6:ITCPTC devices; (D) Electron SCLC and (e) hole SCLC of PM6: Y6: ITCPTC; (F) J_{SC} versus light intensity relationship curves. UV-vis: Ultraviolet-visible; PL: Photoluminescence; J_{SC}: Short-circuit current density; V_{OC}: Open-circuit voltage; SCLC: Space charge limited current; ITCPTC: 3,9-bis{2-methylene-[3-(1,1-dicyanomethylene)-cyclopentane-1,3-dione-(c)thiophen]}-5,5,11,11-tetrakis(4-hexylphenyl)-dithieno[2,3-d:2′,3′-d′]-s-indaceno[1,2-b:5,6-b′]dithiophene; DRS: Diffuse reflectance spectroscopy.

respectively, and that of Y6 is at 950 nm. The PL of Y6: ITCPTC blend film is strongest at 940 nm. Considering that there is no characteristic emission of ITCPTC in the blend film, while there is an enhancement at the emission peak of Y6 and a large overlap with the original peak, this indicates energy transfer between Y6 and ITCPTC[37]. In general, if an efficient charge transfer occurs between two organic semiconductors, then the short-circuit current density (J_{SC}) and the open-circuit voltage (V_{OC}) will be increased. After preparing Y6: ITCPTC into Organic Photovoltaics (OPV) devices, as shown in Figure 2C and Supplementary Table 3, the J-V curves indicated that the J_{SC} of Y6 and Y6: ITCPTC (0.5:0.5) were 0.362 and 0.384 mA/cm^2, respectively, indicating that no significant charge transfer occurred between Y6 and ITCPTC[41]. In summary, there is an energy transfer and no charge transfer between Y6 and ITCPTC. The exciton energy of the third component ITCPTC can be transferred to the receptor Y6 by means of Förster or Dexter energy transfer. That is, the exciton energy produced by the wide bandgap material can be transferred to the narrow bandgap material. We then used the space charge limited current (SCLC) to compare the carrier mobility of the devices with different materials[42]. As shown in Figure 2D and E and Supplementary Table 4, the values of μ_h/μ_e are 1.785, 1.452, and 1.868 with an incremental proportion of ITCPTC, achieving the most balanced charge transport in ternary films. Meanwhile, we examined the correlation between light intensity and current density to gain a better comprehension of the impact of the third component. The fitted slope from Figure 2F indicated lower carrier complexation in ternary films. These results prove that ITCPTC reduces the recombination of electrons and holes in organic semiconductors. Undoubtedly, adding the third component is beneficial to improve photocatalytic performance[42].

Adsorption and photocatalytic properties

The degradation of fluoroquinolone antibiotics by CSC-PM6: Y6: ITCPTC was evaluated using CIP as a contaminant, including adsorption and photocatalytic performance. CSC-PM6: Y6: ITCPTC has certain

adsorption properties, and adsorption experiments were performed in the dark before photodegradation. To assess the adsorption capacity on CIP, pseudo-first-order [Eq. (1)] and pseudo-second-order [Eq. (2)] kinetics models were employed [Figure 3A-C], Langmuir and Freundlich isotherm model [Supplementary Table 5] was developed to assess the adsorption thermodynamic[43,44].

$$\log(q_e - q_t) = \log q_e - \frac{k_1}{2.303} t \quad (1)$$

$$\frac{t}{q_t} = \frac{t}{q_e} + \frac{1}{k_2 q_e^2} \quad (2)$$

Where the k_1 (min^{-1}) and k_2 (L mg^{-1} min^{-1}) denoted the adsorption rate constant of the pseudo-first-order and pseudo-second-order kinetics, respectively. Besides, the q_e (mg/g) is equilibrium adsorption capacity and the q_t (mg/g) is the sorption amount at time t.

The fitting results of CIP adsorption are listed in Supplementary Table 6. The correlation coefficient (R^2) of the pseudo-first-order model (0.9914) is higher than that of the pseudo-second-order model (0.9860), implying that physical adsorption is the restrictive element in the CIP adsorption. To further study the adsorption capacity and adsorption mechanism of CIP by CSC-PM6: Y6: ITCPTC, the relationship between the equilibrium solution concentration (C_e) and the equilibrium adsorption amount (q_e) was investigated using isothermal adsorption model. Langmuir isotherm and Freundlich isotherm are used to analyze the data obtained at different concentrations. As shown in Supplementary Figure 3, the R^2 of Langmuir isotherm was 0.9994, and that of Freundlich isotherm was 0.9950. Langmuir isotherm showed a better description of the isothermal adsorption data, which meant that the adsorption of CIP was single-layer adsorption on a uniform surface with limited adsorption sites. Due to the good correlation between Langmuir and Freundlich isothermal models, the results indicated that the adsorption of CIP on CSC-PM6: Y6: ITCPTC was affected by the single-layer chemisorption and multilayer physical interaction. Good adsorption effect provides abundant reactive sites for photocatalysis, and a large number of surface active sites are more conducive to accelerating the interfacial reaction.

Then, the photodegradation of CIP by CSC-PM6: Y6: ITCPTC was evaluated[45]. Photocatalytic degradation experiments were performed under Xe lamp irradiation (79 mW/cm^2), and as can be seen from Figure 3D, CSC-PM6: Y6: ITCPTC had the best degradation effect, removing 99% of the CIP in 1 h. The photocatalytic performance was quite impressive compared to the references previously published [Supplementary Figure 4, Supplementary Table 7]. To quantitatively evaluate the CIP degradation kinetics, the pseudo-first-order [Eq. (3)] model was employed to fit the data.

$$-\ln\left(\frac{C_t}{C_0}\right) = kt \quad (3)$$

Where the k (min^{-1}) is the degradation rate constant of pseudo-first-order kinetics. C_t and C_0 are the remaining concentrations at reaction time t and initial CIP concentration. The results [Figure 3E] showed that CSC-PM6: Y6: ITCPTC had the largest CIP degradation rate constant (0.05185 min^{-1}), which was consistent with the spectral absorption of photocatalysts. Moreover, the reaction rate of degradation was not positively correlated with concentration when the catalyst concentration was increased [Supplementary Figure 5]. Photocatalysis was inhibited at high catalyst concentrations, probably because excessive solid particles blocked the light absorption of the catalyst, resulting in a lower photoconversion efficiency. At the appropriate concentration, there are enough contact sites between the pollutant and the catalyst, which facilitates the catalytic reaction. In order to determine the mineralization degree of CIP, the Total Organic Carbon (TOC) and Chemical Oxygen Demand (COD) during the degradation were measured. As shown in

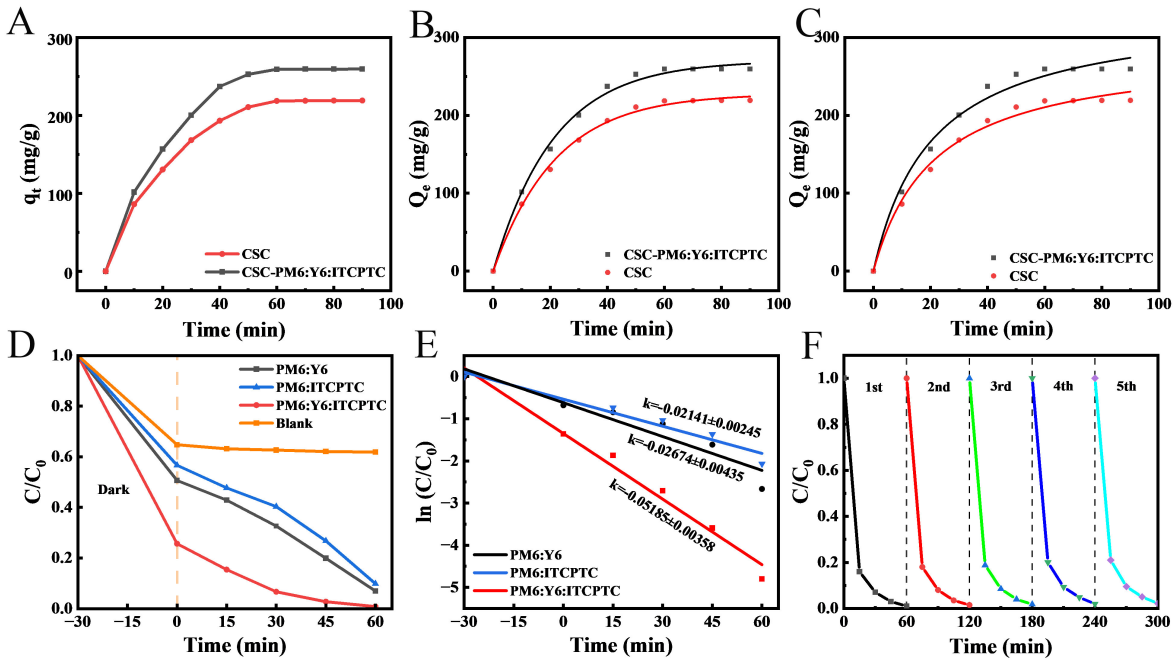

Figure 3. (A) The adsorption of CIP to the CSC and CSC-PM6: Y6:ITCPTC in the dark; (B) the pseudo-first-order model and (C) the pseudo-second-order model for CIP adsorption; (D) Photodegradation of CIP under Xenon lamp; (E) the pseudo-first-order reaction kinetic curve; (F) cyclic stability of PM6: Y6:ITCPTC photocatalyst for five repeated cycles of photodegradation of CIP. CIP: Ciprofloxacin: CSC: Coconut shell carbon; ITCPTC: 3,9-bis{2-methylene-[3-(1,1-dicyanomethylene)-cyclopentane-1,3-dione-(c)thiophen]}-5,5,11,11-tetrakis(4-hexylphenyl)-dithieno[2,3-d:2′,3′-d′]-s-indaceno[1,2-b:5,6-b′]dithiophene.

Supplementary Figure 6, the pollutants are basically mineralized after 60 minutes of reaction. Subsequently, photocatalysis was carried out under indoor light conditions (1 mW/cm^2) and it was found that the degradation rate of CIP could also reach 90% in 1 h [Supplementary Figure 7]. This result showed that the photocatalyst can still exhibit good photocatalytic performance even under weak light intensity, which provided a new possibility to solve the problem of antibiotic pollution in the environment. The addition of the third component ITCPTC effectively improved the photodegradation efficiency[46]. After the photodegradation experiments, the stability of CSC-PM6: Y6: ITCPTC was evaluated by cycling experiments. As shown in Figure 3F, the degradation rate only decreased by 1.22% after five cycles, and there was no significant change in the morphology and structure of the catalyst [Supplementary Figures 8 and 9], implying that CSC-PM6: Y6: ITCPTC had good stability. And after experiencing dozens of cyclic experiments, it could still maintain high photocatalytic performance. The above results indicated that CSC-PM6: Y6: ITCPTC had good photocatalytic degradation performance. The possible reasons why the photocatalytic degradation of CIP can be enhanced by using ternary organic photocatalysts are[47]: (1) the introduction of the third component, ITCPTC, broadens the light absorption range and enhances light harvesting; (2) The existence of energy transfer between the two receptors favors the enhancement of charge transport.

Optoelectronic properties of photocatalysts

After determining the excellent photocatalytic activity of CSC-PM6: Y6: ITCPTC, the photoelectric properties of the prepared photocatalysts were studied to elucidate the factors contributing to their outstanding photocatalytic performance. The photovoltaic performance of the catalysts was evaluated by PL, time-resolved PL (TRPL), electrochemical impedance spectroscopy (EIS) and photocurrent density. The separation and recombination of carriers were investigated by PL spectroscopy. Typically, the higher the PL

peak, the higher carriers recombination rate and the lower the separation efficiency. As shown in Figure 4A, CSC-PM6: Y6: ITCPTC presented lower PL intensity, which indicated that the ternary bulk-heterojunction made the separation of the carriers more effective. This characteristic suggested that the ternary system possesses a lower carrier recombination rate and better carrier separation compared to the binary system. TRPL spectrum was shown in Figure 4B The average decay lifetime was 1.61 ns, 1.64 ns, and 2.15 ns for PM6: Y6, PM6: ITCPTC and PM6: Y6: ITCPTC, respectively. The longer carrier lifetime of CSC-PM6: Y6: ITCPTC can indicate its superior charge transfer performance. These results implied less non-radiative recombination and better charge transport performance in CSC-PM6: Y6: ITCPTC.

To further examine the charge transfer properties, the EIS was employed to test photocatalysts. As displayed in Figure 4C, the arc radius of CSC-PM6: Y6: ITCPTC was the smallest. In general, a smaller arc radius implies higher carrier transport efficiency. Therefore, the low impedance of CSC-PM6: Y6: ITCPTC indicates that it has the lowest carrier migration resistance and the best charge transfer ability. It can be observed by photocurrent test that CSC-PM6: Y6: ITCPTC exhibited superior photocurrent intensity [Figure 4D]. CSC-PM6: Y6: ITCPTC can generate stronger photocurrent, and the current density trend was consistent with EIS. According to the results of the above photoelectric tests, it can be inferred that the formation of the PM6: Y6: ITCPTC heterojunction has improved the photoelectric effect of the photocatalyst, thereby enhancing its photocatalytic performance., and the introduction of the third component enhances the separation of electron-hole pairs[48].

Photocatalytic degradation mechanism

To investigate the active species for CIP degradation, the scavenger tests were conducted by adding t-BQ, EDTA-2Na, and IPA as scavengers of superoxide radical ($\cdot O_2^-$), hole (h^+) and hydroxyl radical (·OH), respectively[49]. As shown in Figure 5A, when t-BQ was added, the photodegradation rate of CIP dropped sharply to only 53.6%, while in the presence of EDTA-2Na and IPA, the corresponding photodegradation rates of CIP decreased to 66.1% and 82%, respectively. The above results suggested that the primary free radicals in the CIP degradation system were $\cdot O_2^-$ and h^+. Then, to verify the presence of free radicals, the ESR analysis for $\cdot O_2^-$, h^+ and ·OH detection was performed. 5,5-Dimethyl-1-pyrroline N-oxide (DMPO) was used to detect the presence of $\cdot O_2^-$ and ·OH in methanol and superhydrophobic dispersions, respectively. As shown in Figure 5B and C, no electrostatic surface potential (ESP^-) and DMPO-·OH signals appeared under dark conditions, and the signals were clear when visible light was irradiated for 5min, and the intensity of the signals increased slightly after 10min of light irradiation. Meanwhile, 2,2,6,6-Tetramethylpiperidine-1-oxyl (TEMPO) was used as h^+ trapping agent. Since TEMPO is a paramagnetic substance with ESR signal under dark conditions, the electrons generated by the catalyst can reduce TEMPO to obtain non-paramagnetic 1-Hydroxy-2,2,6,6-tetramethylpiperidine (TEMPOH) under illumination, and the reduction of ESR signal can prove the generation of electron-hole pairs. As shown in Figure 5D, the signal was clear in dark conditions, and the intensity decreased with the extension of time. The results of ESR analysis confirmed that CSC-PM6: Y6: ITCPTC system produced ROSs in the photocatalytic process, suggesting that $\cdot O_2^-$, h^+ and ·OH were involved in the photocatalytic degradation of CIP. These results were also consistent with the experimental results of free radical trapping experiments.

In order to further understand the photogenerated charge behavior at photocatalyst interfaces, we applied surface photovoltaic methods to investigate the separation and transport of photogenerated carriers, and Figure 6A showed the surface photovoltage (SPV) spectrum of catalyst PM6: Y6: ITCPTC (1:1:0, 1:0.5:0.5). From the SPV signals under Xe lamp irradiation, it can be seen that the photovoltage of the photocatalyst PM6: Y6: ITCPTC was significantly higher than that of the photocatalyst PM6: Y6, implying that the charge separation efficiency of the ternary photocatalyst was higher. Meanwhile, at wavelength < 700 nm, the photovoltaic signal of the catalyst was positive, indicating that photogenerated electrons migrated towards

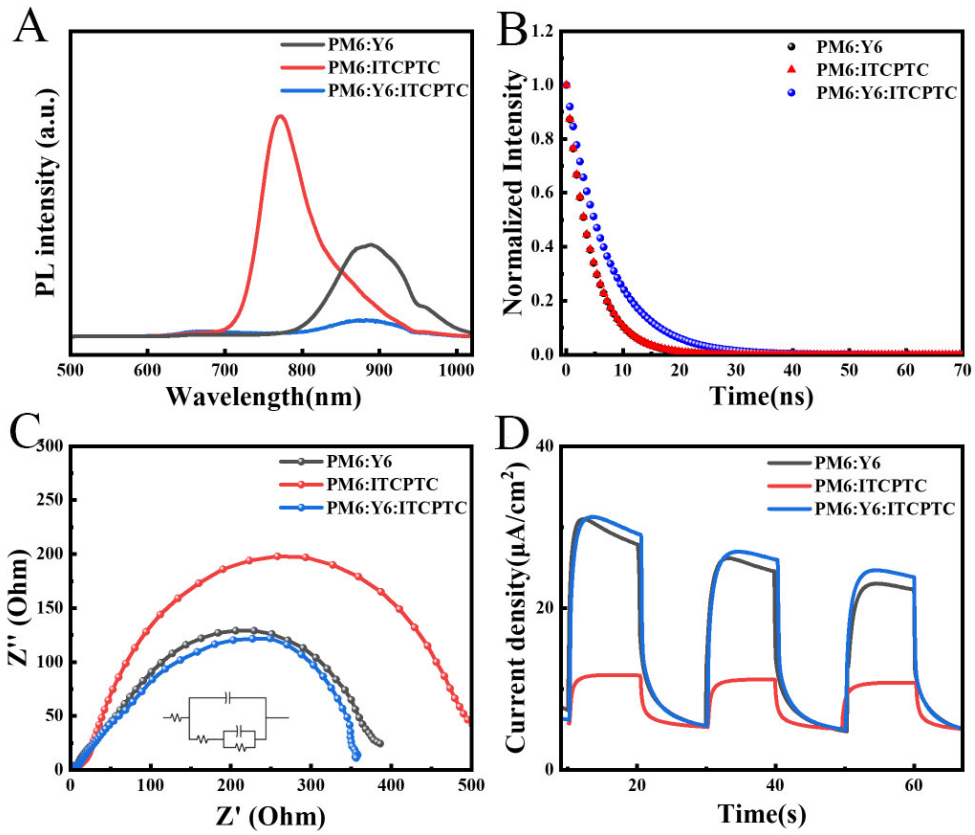

Figure 4. (A) Photoluminescence spectra; (B) TRPL spectra; (C) EIS plots and (D) Photocurrent response densities of the PM6: Y6:ITCPTC (1:1:0, 1:0:1, 1:0.5:0.5). EIS: Electrochemical impedance spectroscopy; TRPL: Time-resolved photoluminescence; PL: Photoluminescence; ITCPTC: 3,9-bis{2-methylene-[3-(1,1-dicyanomethylene)-cyclopentane-1,3-dione-(c)thiophen]}-5,5,11,11-tetrakis(4-hexylphenyl)-dithieno[2,3-d:2′,3′-d′]-s-indaceno[1,2-b:5,6-b′]dithiophene.

the bulk phase in the presence of a surface built-in field when PM6 was excited, and the photogenerated holes accumulated on the PM6 surface. At wavelength > 700 nm, the photovoltaic signal of the catalyst was negative, indicating that photogenerated electrons migrated towards the surface in the presence of a surface built-in field when Y6 was excited, and the photogenerated electrons accumulated on the Y6 surface. This also showed that the direction of the interfacial electric field was pointing from PM6 to Y6, and under the action of the interfacial electric field, the photogenerated electrons were shifted into Y6, while the photogenerated holes remained in PM6. Based on the behavior of photogenerated charges, we can confirm that the bulk-heterojunction formed by PM6: Y6 was type- II heterojunction [Figure 6A], and the formation of the type-II heterojunction facilitated the separation and transfer of photogenerated carriers, thus achieving superior photocatalytic performance.

Based on the above, the mechanism for photodegradation of CIP by CSC-PM6: Y6: ITCPTC was proposed and presented in Figure 6B. According to the band structure of PM6, Y6 and ITCPTC, PM6 and Y6 have staggered bands to provide a driving force for charge separation and transport[50]. When PM6: Y6 absorbs light energy from light source, both components generate photogenerated electrons (e^-) and holes (h^+). Photogenerated electrons from the donor PM6 E_{LUMO} are transferred to the acceptor Y6 E_{LUMO}, while the holes from Y6 E_{HOMO} are transferred to PM6 E_{HOMO}. When adding the third component ITCPTC, due to the direct charge transfer between narrow gap acceptor Y6 and wide gap acceptor ITCPTC, the exciton energy generated in ITCPTC can be transferred to Y6, and the excitons dissociate at the PM6/Y6 interface[33,51]. At

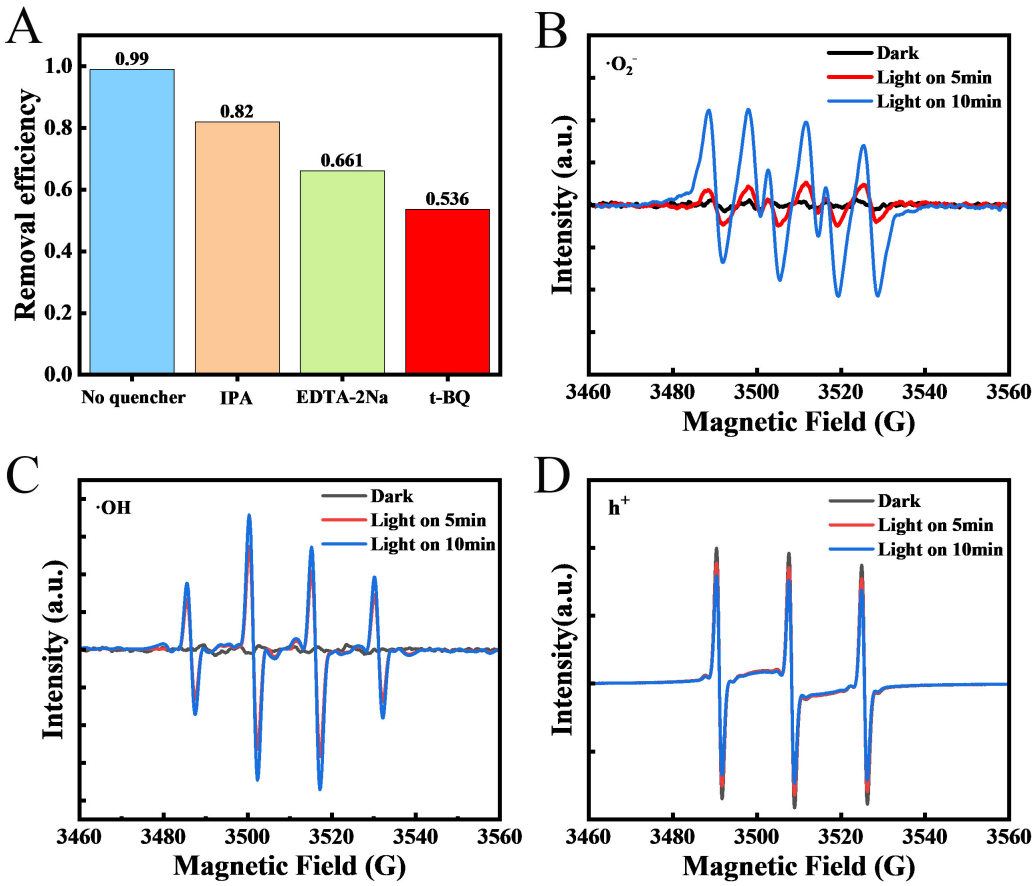

Figure 5. (A) Scavenger experiments on photodegradation of CIP. The ESR spectra with PM6: Y6:ITCPTC for (B) DMPO-·O_2^-; (C) DMPO-·OH and (D) TEMPO-h^+ under illumination. CIP: Ciprofloxacin; ESR: Electron spin resonance; ITCPTC:3,9-bis{2-methylene-[3-(1,1-dicyanomethylene)-cyclopentane-1,3-dione-(c)thiophen]}-5,5,11,11-tetrakis(4-hexylphenyl)-dithieno[2,3-d:2′,3′-d′]-s-indaceno[1,2-b:5,6-b′]dithiophene; DMPO: 5,5-Dimethyl-1-pyrroline N-oxide; TEMPO: 2,2,6,6-Tetramethylpiperidine-1-oxyl.

this time, the addition of the third component can make the system obtain more photon energy, and enhance the charge transfer ability of the photocatalyst[19]. This also confirms that the photocatalytic performance of the ternary system is better than that of the binary system. Additionally, ESR analysis of the CSC-PM6: Y6: ITCPTC photocatalyst revealed that the material generated h^+, $\cdot O_2^-$ and ·OH under visible light. The results showed that e^- and O_2 produced $\cdot O_2^-$, h^+ and H_2O produced ·OH, and participated in the degradation of CIP. Meanwhile, the h^+ accumulated on E_{HOMO} of PM6 can directly oxidize part of CIP because of its considerable oxidizing ability. As a result, the photocatalytic performance of CIP is significantly promoted. The possible photodegradation mechanism is proposed as follows:

$$\text{PM6: Y6: ITCPTC} + h\nu \rightarrow \text{PM6: Y6: ITCPTC} \left(e_{LUMO}^- + h_{HOMO}^+\right) \quad (4)$$

$$e_{LUMO}^- + O_2 \rightarrow \cdot O_2^- \quad (5)$$

$$h_{HOMO}^+ + H_2O \rightarrow H^+ + \cdot OH \quad (6)$$

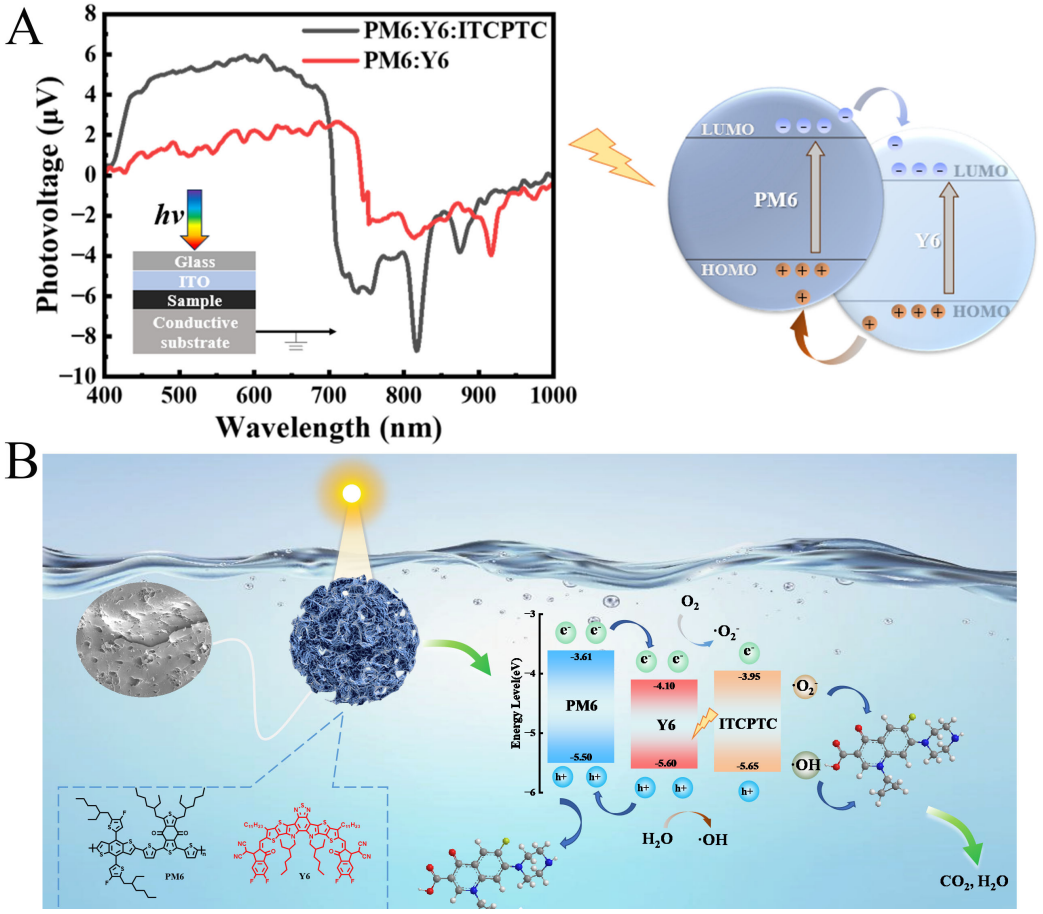

Figure 6. (A) SPV spectrum of PM6: Y6: ITCPTC heterostructure film; (B) Photocatalytic degradation mechanism of CIP by CSC-PM6: Y6: ITCPTC under visible light irradiation. SPV: Showed the surface photovoltage; CIP: Ciprofloxacin; CSC: Coconut shell carbon; HOMO: Highest occupied molecular orbital; LUMO: Lowest unoccupied molecular orbital; ITCPTC: 3,9-bis{2-methylene-[3-(1,1-dicyanomethylene)-cyclopentane-1,3-dione-(c)thiophen]}-5,5,11,11-tetrakis(4-hexylphenyl)-dithieno[2,3-d:2′,3′-d′]-s-indaceno[1,2-b:5,6-b′]dithiophene.

$$h_{HOMO}^{+} + OH^{-} \rightarrow \cdot OH \quad (7)$$

$$\text{Pollutants} + \text{Active species } (e_{LUMO}^{-}, h_{HOMO}^{+}, \cdot O_2^{-}, \cdot OH) \rightarrow CO_2 + H_2O \quad (8)$$

Degradation pathway of CIP

Liquid chromatography-mass spectrometry (LC-MS) was utilized to analyze the intermediate products and degradation pathways of CIP. Based on fragment spectra, the intermediate products at various reaction times were identified[52]. As shown in Supplementary Figure 10, peaks of different mass spectra were detected after 15 and 30 minutes of visible light irradiation, indicating that CIP has been broken down into intermediates. Based on density functional theory (DFT) calculation, the Electrostatic Surface Potential (ESP) and the Fukui function were introduced to further investigate the photodegradation pathway of CIP. As shown in Figure 7A, the ESP diagram of CIP indicated that the piperazine ring could easily bind to the negatively charged $\cdot O_2^-$. The Fukui function calculations were showed in Supplementary Figure 11. Electrophilic and nucleophilic radicals tended to attack atoms with higher f^- and f^+ values, respectively.

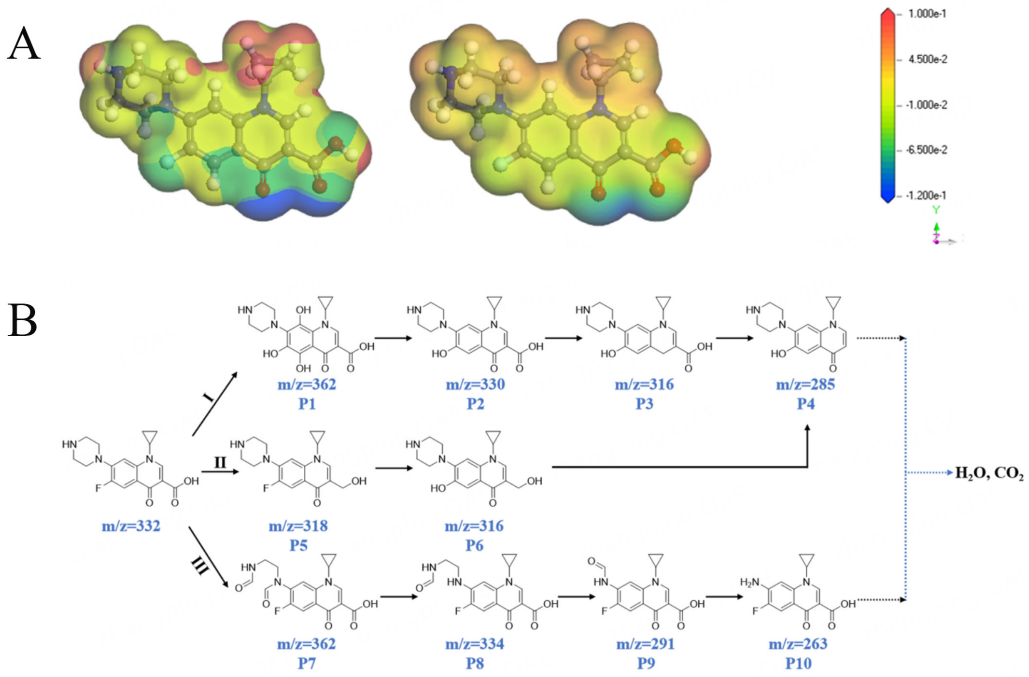

Figure 7. (A) Electrostatic potential (ESP) diagram of CIP; (B) Possible photodegradation pathways of CIP. ESP: Electrostatic Surface Potential; CIP: Ciprofloxacin.

According to the above calculations, nitrogen in the piperazine ring, the fluorine atom and the carboxyl group were the most active sites.

According to the LC-MS and DFT calculation, possible photodegradation pathways of CIP have been inferred as shown in Figure 7B. The photodegradation pathways of CIP by CSC-PM6: Y6: ITCPTC might be defluorination (Figure 7B, pathway I), decarboxylation (Figure 7B pathway II) and piperazine ring cleavage (Figure 7B, pathway III). In pathway I, photodegradation of CIP began with the substitution of fluorine (-F) by hydroxyl group (-OH), causing the generation of P1 (m/z=362); then the hydroxyl group of P1 was attacked, generating intermediate P2 (m/z=330). Subsequently, decarboxylation reaction occurred to generate P3 (m/z=316). In pathway II, CIP produced intermediate P5 (m/z=318) through decarboxylation, followed by the substitution of fluorine to generate P6 (m/z=316). Pathway III was the oxidation of piperazine side chain caused by free radical attacking; the C-N between piperazine ring and benzene was attacked by h^+ to generate P7 (m/z=362). The P7 lost an aldehyde group to form P8 (m/z=334). P8 then (m/z=334) lost secondary amine nitrogen and underwent oxidation to generate P9 (m/z=291), which subsequently lost amine side chain formaldehyde to generate P10 (m/z=263). Since $\cdot O_2^-$ and h^+ played a major role in the photodegradation of CIP, it can be inferred from the ESP and Fukui function calculations that the piperazine ring was more susceptible to being attacked in the presence of these free radicals. Then, piperazine ring opened by oxidation. On the other hand, considering the effect of potential energy, the substitution of -F was thermodynamically unfavorable to perform. After calculating the activation energy of different reaction pathways [Supplementary Figure 12, Supplementary Table 8], the activation energy of pathway II was relatively low. By comparison, pathways II and III represented a more advantageous reaction route. Finally, these intermediates were degraded into small molecules by ROSs and eventually were degraded into H_2O and CO_2.

CONCLUSIONS

In this work, we developed an improved visible-light-driven photocatalyst, CSC-PM6: Y6: ITCPTC, by loading the organic semiconductors to CSC to degrade CIP. For the first time, the donor and acceptor of organic photovoltaic active layers have been applied to the field of photocatalysis, signifying a breakthrough. The photodegradation efficiency of CIP reached 99% under light irradiation within 60 min, which is currently the best reported efficiency of a pure organic photocatalytic system for the degradation of CIP. CSC-PM6: Y6: ITCPTC had a higher k value (k = 0.05185 min^{-1}) than PM6: Y6 and PM6: ITCPTC. The use of a ternary system can effectively improve the charge transfer efficiency, reduce the recombination between electron-hole pairs, and widen the light absorption, thereby enhancing the photocatalytic performance. The main active species that played a role in the photodegradation process were h^+ and $\cdot O_2^-$. Meanwhile, based on DFT calculation and experimental results, three possible CIP photodegradation pathways were inferred. The catalyst solves the problems of short service life and high cost of traditional catalysts, and has extremely high stability and recyclability. Building on this advanced and inspiring performance of the catalyst, this work offers a new suitable way to treat organic pollutants in water environments, and emphasizes the significance of photocatalysis by adjusting the light utilization and photoelectric performance of organic semiconductors.

DECLARATIONS

Authors' contributions

Conceptualization, methodology: Zhou, Y.; Liu, T.
Writing - original draft, experimental, data analysis: Zhou, Y.
Writing - review and editing: Zhou, Y.; Huang, C.; Liu, T.
Visualization, software: Yang, L.; Zhang, R.; Liu, C.; Li, L.; Sun, K.; Yao, S.; Geng, N.; Luo, Y.
Funding acquisition: Yang, T.; Zou B.; Liu, T.
Supervision: Yin, Y.; Liu, T.

Availability of data and materials

Data will be made available upon reasonable request to the corresponding author.

Financial support and sponsorship

This work was supported by Guangxi NSF project (2020GXNSFDA238004), the Scientific and Technological Bases and Talents of Guangxi (Guike AD21238027), Guangxi Science and Technology Major Program (Guike AA24206037), the special fund for "Guangxi Bagui Scholars", the Training Project of High-level Professional and Technical Talents of Guangxi University and Natural Science and Technology Innovation Development Multiplication Program of Guangxi University (2022BZRC006), PTDC/EME-REN/1497/2021, UIDB/00481/2020 and UIDP/00481/2020 - Fundação para a Ciência e a Tecnologia; and CENTRO-01-0145-FEDER-022083 - Centro Portugal Regional Operational Programme (Centro2020), under the PORTUGAL 2020 Partnership Agreement, through the European Regional Development Fund.

Conflicts of interest

All authors declared that there are no conflicts of interest.

Ethical approval and consent to participate

Not applicable.

Consent for publication

Not applicable.

REFERENCES

1. Greenwood, D.; Laverick, A. Activities of newer quinolones against *Legionella* group organisms. *Lancet* **1983**, *2*, 279-80. DOI PubMed
2. D'Costa, V. M.; McGrann, K. M.; Hughes, D. W.; Wright, G. D. Sampling the antibiotic resistome. *Science* **2006**, *311*, 374-7. DOI PubMed
3. Bobu, M.; Yediler, A.; Siminiceanu, I.; Schulte-hostede, S. Degradation studies of ciprofloxacin on a pillared iron catalyst. *Appl. Catal. B:. Environ.* **2008**, *83*, 15-23. DOI
4. Davies, J.; Davies, D. Origins and evolution of antibiotic resistance. *Microbiol. Mol. Biol. Rev.* **2010**, *74*, 417-33. DOI PubMed PMC
5. Vieno, N. M.; Härkki, H.; Tuhkanen, T.; Kronberg, L. Occurrence of pharmaceuticals in river water and their elimination in a pilot-scale drinking water treatment plant. *Environ. Sci. Technol.* **2007**, *41*, 5077-84. DOI
6. Watkinson, A. J.; Murby, E. J.; Costanzo, S. D. Removal of antibiotics in conventional and advanced wastewater treatment: implications for environmental discharge and wastewater recycling. *Water. Res.* **2007**, *41*, 4164-76. DOI PubMed
7. Yang, T.; Peng, J.; Zheng, Y.; et al. Enhanced photocatalytic ozonation degradation of organic pollutants by ZnO modified TiO_2 nanocomposites. *Appl. Catal. B:. Environ.* **2018**, *221*, 223-34. DOI
8. An, T.; Yang, H.; Li, G.; Song, W.; Cooper, W. J.; Nie, X. Kinetics and mechanism of advanced oxidation processes (AOPs) in degradation of ciprofloxacin in water. *Appl. Catal. B:. Environ.* **2010**, *94*, 288-94. DOI
9. Zheng, N.; Li, L.; Tang, X.; et al. Spontaneous formation of low valence copper on red phosphorus to effectively activate molecular oxygen for advanced oxidation process. *Environ. Sci. Technol.* **2023**, *57*, 5024-33. DOI
10. Gong, X.; Song, P.; Han, C.; Xiao, Y.; Mei, X.; Xu, W. Heterogeneous single-atom catalysts for energy process: recent progress, applications and challenges. *Energy. Mater.* **2023**, *3*, 300016. DOI
11. Schneider, J.; Matsuoka, M.; Takeuchi, M.; et al. Understanding TiO_2 photocatalysis: mechanisms and materials. *Chem. Rev.* **2014**, *114*, 9919-86. DOI
12. Hu, X.; Hu, X.; Peng, Q.; et al. Mechanisms underlying the photocatalytic degradation pathway of ciprofloxacin with heterogeneous TiO_2. *Chem. Engg. J.* **2020**, *380*, 122366. DOI
13. Liccardo, L.; Bordin, M.; Sheverdyaeva, P. M.; et al. Surface defect engineering in colored TiO_2 hollow spheres toward efficient photocatalysis. *Adv. Funct. Mater.* **2023**, *33*, 2212486. DOI
14. Gogoi, D.; Karmur, R. S.; Das, M. R.; Ghosh, N. N. Cu and $CoFe_2O_4$ nanoparticles decorated hierarchical porous carbon: an excellent catalyst for reduction of nitroaromatics and microwave-assisted antibiotic degradation. *Appl. Catal. B:. Environ.* **2022**, *312*, 121407. DOI
15. Yang, L.; Peng, Y.; Luo, X.; et al. Beyond C_3N_4 π-conjugated metal-free polymeric semiconductors for photocatalytic chemical transformations. *Chem. Soc. Rev.* **2021**, *50*, 2147-72. DOI
16. Yang, C.; Wang, J.; Wang, R.; et al. Efficient hollow cubic Co_9S_8@defective ZnS/g-C_3N_4 for multi-pollutants removal via cascade Z-scheme heterojunction. *Appl. Catal. B:. Environ.* **2023**, *322*, 122084. DOI
17. Sun, Q.; Wang, N.; Yu, J.; Yu, J. C. A hollow porous CdS photocatalyst. *Adv. Mater.* **2018**, *30*, e1804368. DOI
18. Yang, J.; Miao, H.; Jing, J.; Zhu, Y.; Choi, W. Photocatalytic activity enhancement of PDI supermolecular via π-π action and energy level adjusting with graphene quantum dots. *Appl. Catal. B:. Environ.* **2021**, *281*, 119547. DOI
19. Chen, R.; Fan, F.; Dittrich, T.; Li, C. Imaging photogenerated charge carriers on surfaces and interfaces of photocatalysts with surface photovoltage microscopy. *Chem. Soc. Rev.* **2018**, *47*, 8238-62. DOI PubMed
20. Gao, Q.; Xu, J.; Wang, Z.; Zhu, Y. Enhanced visible photocatalytic oxidation activity of perylene diimide/g-C_3N_4 n-n heterojunction via π-π interaction and interfacial charge separation. *Appl. Catal. B:. Environ.* **2020**, *271*, 118933. DOI
21. Safira, A. R.; Alluhayb, A. H.; Aadil, M.; Alkaseem, M.; Fattah-alhosseini, A.; Kaseem, M. Enhanced photocatalytic reduction of p-nitrophenol by polyvinylpyrrolidone-modified MOF/porous MgO composite heterostructures. *Compos. Part. B:. Eng.* **2024**, *284*, 111710. DOI
22. Fang, Y.; Hou, Y.; Fu, X.; Wang, X. Semiconducting polymers for oxygen evolution reaction under light illumination. *Chem. Rev.* **2022**, *122*, 4204-56. DOI
23. Lu, F.; Fu, S.; Wang, L.; et al. Enhanced performance of inverted polymer solar cells by adding benzyl viologen dichloride into ZnO electron transport layer. *Opt. Mater.* **2023**, *139*, 113782. DOI
24. Sun, R.; Wu, Q.; Guo, J.; et al. A layer-by-layer architecture for printable organic solar cells overcoming the scaling lag of module efficiency. *Joule* **2020**, *4*, 407-19. DOI
25. Cai, S.; Huang, C.; Wang, C.; et al. New breakthrough in dye removal: ultrafast removal of high concentration MB with biochar-based organic photocatalysts under indoor light (30W/m^2) drive. *J. Clean. Prod.* **2024**, *449*, 141539. DOI
26. Liang, Y.; Zhang, L.; Huang, C.; et al. New breakthrough in rapid degradation of lignin derivative compounds · a novel high stable and reusable green organic photocatalyst. *J. Colloid. Interface. Sci.* **2024**, *662*, 426-37. DOI
27. Zhang, W.; Zhang, L.; Luo, H.; et al. Organic heterojunctions synergize with biochar as catalytic sites for rapid herbicide degradation under natural light. *Surf. Interfaces.* **2024**, *46*, 104182. DOI

28. Xie, D.; Liu, T.; Gao, W.; et al. A novel thiophene-fused ending group enabling an excellent small molecule acceptor for high-performance fullerene-free polymer solar cells with 11.8% efficiency. *Sol. RRL.* **2017**, *1*, 1700044. DOI
29. Yan, T.; Song, W.; Huang, J.; Peng, R.; Huang, L.; Ge, Z. 16.67% rigid and 14.06% flexible organic solar cells enabled by ternary heterojunction strategy. *Adv. Mater.* **2019**, *31*, e1902210. DOI
30. Ma, R.; Liu, T.; Luo, Z.; et al. Improving open-circuit voltage by a chlorinated polymer donor endows binary organic solar cells efficiencies over 17%. *Sci. China. Chem.* **2020**, *63*, 325-30. DOI
31. Qi, Q.; Ke, H.; Ye, L. Ternary organic solar cells featuring polythiophene. *Energy. Mater.* **2022**, *2*, 35. DOI
32. Xiao, Y.; Feng, C.; Fu, J.; et al. Band structure engineering and defect control of Ta_3N_5 for efficient photoelectrochemical water oxidation. *Nat. Catal.* **2020**, *3*, 932-40. DOI
33. Ye, J. H.; Bellotti, P.; Heusel, C.; Glorius, F. Photoredox-catalyzed defluorinative functionalizations of polyfluorinated aliphatic amides and esters. *Angew. Chem. Int. Ed. Engl.* **2022**, *61*, e202115456. DOI PubMed
34. Bellotti, P.; Huang, H. M.; Faber, T.; Glorius, F. Photocatalytic late-stage C-H functionalization. *Chem. Rev.* **2023**, *123*, 4237-352. DOI PubMed
35. Chen, X.; Zhao, J.; Li, G.; Zhang, D.; Li, H. Recent advances in photocatalytic renewable energy production. *Energy. Mater.* **2022**, *2*, 200001. DOI
36. Zhang, M.; Gao, W.; Zhang, F.; et al. Efficient ternary non-fullerene polymer solar cells with PCE of 11.92% and FF of 76.5%. *Energy. Environ. Sci.* **2018**, *11*, 841-9. DOI
37. Ma, R.; Liu, T.; Luo, Z.; et al. Adding a third component with reduced miscibility and higher LUMO level enables efficient ternary organic solar cells. *ACS. Energy. Lett.* **2020**, *5*, 2711-20. DOI
38. Liu, T.; Luo, Z.; Fan, Q.; et al. Use of two structurally similar small molecular acceptors enabling ternary organic solar cells with high efficiencies and fill factors. *Energy. Environ. Sci.* **2018**, *11*, 3275-82. DOI
39. Wang, F.; Feng, Y.; Chen, P.; et al. Photocatalytic degradation of fluoroquinolone antibiotics using ordered mesoporous g-C_3N_4 under simulated sunlight irradiation: kinetics, mechanism, and antibacterial activity elimination. *Appl. Catal. B:. Environ.* **2018**, *227*, 114-22. DOI
40. Liu, F.; Zhou, L.; Liu, W.; et al. Organic solar cells with 18% efficiency enabled by an alloy acceptor: a two-in-one strategy. *Adv. Mater.* **2021**, *33*, e2100830. DOI
41. Liu, T.; Yang, T.; Ma, R.; et al. 16% efficiency all-polymer organic solar cells enabled by a finely tuned morphology via the design of ternary blend. *Joule* **2021**, *5*, 914-30. DOI
42. Liu, X.; Peng, Y.; Liang, Z.; et al. Efficient ternary organic photovoltaic device with a non-halogenated solvent *via* synergistic inhibiting charge recombination and regulating morphology. *J. Mater. Chem. C.* **2023**, *11*, 2871-9. DOI
43. Zhang, M.; Zhang, Y.; Zhu, Y.; et al. Insights into adsorption and high photocatalytic oxidation of ciprofloxacin under visible light by intra-molecular donor-acceptor like p-n isotype heterojunction: performance and mechanism. *Chem. Eng. J.* **2023**, *464*, 142533. DOI
44. Khan M, Khalid M, Shahid M. What triggers dye adsorption by metal organic frameworks? *Mater. Adv.* **2020**, *1*, 1575-601. DOI
45. Sturini, M.; Speltini, A.; Maraschi, F.; et al. Photodegradation of fluoroquinolones in surface water and antimicrobial activity of the photoproducts. *Water. Res.* **2012**, *46*, 5575-82. DOI
46. Wang, Z.; Li, C.; Domen, K. Recent developments in heterogeneous photocatalysts for solar-driven overall water splitting. *Chem. Soc. Rev.* **2019**, *48*, 2109-25. DOI
47. He, S.; Zhai, C.; Fujitsuka, M.; et al. Femtosecond time-resolved diffuse reflectance study on facet engineered charge□carrier dynamics in Ag_3PO_4 for antibiotics photodegradation. *Appl. Catal. B:. Env.* **2021**, *281*, 119479. DOI
48. Lu, Z.; Peng, J.; Song, M.; et al. Improved recyclability and selectivity of environment-friendly MFA-based heterojunction imprinted photocatalyst for secondary pollution free tetracycline orientation degradation. *Chem. Eng. J.* **2019**, *360*, 1262-76. DOI
49. Doorslaer X, Heynderickx PM, Demeestere K, Debevere K, Van Langenhove H, Dewulf J. TiO_2 mediated heterogeneous photocatalytic degradation of moxifloxacin: operational variables and scavenger study. *Appl. Catal. B:. Environ.* **2012**, *111-112*, 150-6. DOI
50. Su, Q.; Li, J.; Wang, B.; Li, Y.; Hou, L. Direct Z-scheme Bi_2MoO_6/UiO-66-NH_2 heterojunctions for enhanced photocatalytic degradation of ofloxacin and ciprofloxacin under visible light. *Appl. Catal. B:. Environ.* **2022**, *318*, 121820. DOI
51. Hao, X.; Zhou, J.; Cui, Z.; Wang, Y.; Wang, Y.; Zou, Z. Zn-vacancy mediated electron-hole separation in ZnS/g-C_3N_4 heterojunction for efficient visible-light photocatalytic hydrogen production. *Appl. Catal. B:. Environ.* **2018**, *229*, 41-51. DOI
52. Wei, X.; Chen, J.; Xie, Q.; Zhang, S.; Ge, L.; Qiao, X. Distinct photolytic mechanisms and products for different dissociation species of ciprofloxacin. *Environ. Sci. Technol.* **2013**, *47*, 4284-90. DOI